arXiv:2306.03991v1 [astro-ph.SR] 6 Jun 2023

Numerical evidence for a small-scale dynamo approaching solar magnetic Prandtl numbers

Jörn Warnecke[1*], Maarit J. Korpi-Lagg[2,1,3], Frederick A. Gent[2,4] and Matthias Rheinhardt[2]

[1*]Max-Planck-Institut für Sonnensystemforschung, Justus-von-Liebig-Weg 3, Göttingen, D-37077, Germany.
[2]Department of Computer Science, Aalto University, PO Box 15400, Espoo, FI-00 076, Finland.
[3]Nordita, KTH Royal Institute of Technology & Stockholm University, Hannes Alfvéns väg 12, Stockholm, SE-11419, Sweden.
[4]School of Mathematics, Statistics and Physics, Newcastle University, Newcastle upon Tyne, NE1 7RU, UK.

*Corresponding author(s). E-mail(s): warnecke@mps.mpg.de;

Abstract

Magnetic fields on small scales are ubiquitous in the universe. Though they can often be observed in detail, their generation mechanisms are not fully understood. One possibility is the so-called small-scale dynamo (SSD). Prevailing numerical evidence, however, appears to indicate that an SSD is unlikely to exist at very low magnetic Prandtl numbers (Pr_M) such as are present in the Sun and other cool stars. We have performed high-resolution simulations of isothermal forced turbulence employing the lowest Pr_M values so far achieved. Contrary to earlier findings, the SSD turns out to be not only possible for Pr_M down to 0.0031, but even becomes increasingly easier to excite for Pr_M below $\simeq 0.05$. We relate this behaviour to the known hydrodynamic phenomenon referred to as the bottleneck effect. Extrapolating our results to solar values of Pr_M indicates that an SSD would be possible under such conditions.

Astrophysical flows are considered to be susceptible to two types of dynamo instabilities. Firstly, a large-scale dynamo (LSD) is excited by flows exhibiting

helicity, or more generally, lacking mirror-symmetry, due to rotation, shear, and/or stratification. It generates coherent, dynamically significant, magnetic fields on the global scales of the object in question [1]. Characteristics of LSDs vary depending on the dominating generative effects, such as differential rotation in the case of the Sun. Convective turbulence provides both generative and dissipative effects [2], and their presence and astrophysical relevance is no longer strongly debated.

The presence of the other type of dynamo instability, namely the small-scale or fluctuation dynamo (SSD), however, remains controversial in solar and stellar physics. In an SSD-active system, the magnetic field is generated at scales comparable to, or smaller than the characteristic scales of the turbulent flow, enabled by chaotic stretching of field lines at high magnetic Reynolds number [3]. In contrast to the LSD, excitation of an SSD requires significantly stronger turbulence [1]. Furthermore, it has been theorized that it becomes more difficult to excite SSD at very low magnetic Prandtl number Pr_M [4–10], the ratio of kinematic viscosity ν and magnetic diffusivity η. In the Sun, Pr_M can reach values as low as 10^{-6}–10^{-4} [11], thus seriously repudiating whether an SSD can at all be present. Numerical models of SSD in near-surface solar convection typically operate at $Pr_M \approx 1$ [12–18] and thus circumvent the issue of low-Pr_M dynamos.

A powerful SSD may potentially have a large impact on the dynamical processes in the Sun. It can, for example, influence the angular momentum transport and therefore the generation of differential rotation [19, 20], interact with the LSD [21–25] or contribute to coronal heating via enhanced photospheric Poynting flux [26]. Hence, it is of great importance to clarify whether or not an SSD can exist in the Sun. Observationally, it is still debated whether the small-scale magnetic field on the surface of the Sun has contributions from the SSD or is solely due to the tangling of the large-scale magnetic field by the turbulent motions [27–32]. However, these studies show a slight preference of the small-scale fields to be cycle-independent. SSD at small Pr_M are also important for the interiors of planets and for liquid metal experiments [33].

Various numerical studies have reported increasing difficulties in exciting the SSD when decreasing Pr_M [6, 10, 34], confirming the theoretical predictions. However, current numerical models reach only $Pr_M = 0.03$ using explicit physical diffusion or slightly lower (estimated) Pr_M, relying on artificial hyperdiffusion [7, 8]. To achieve even lower Pr_M, one needs to increase the grid resolution massively, see also [35]. Exciting the SSD requires a magnetic Reynolds number (Re_M) typically larger than 100; hence, e.g., $Pr_M = 0.01$ implies a fluid Reynolds number $Re = 10^4$, where $Re = u_{rms}\ell/\nu$, u_{rms} being the volume integrated root-mean-squared velocity, ℓ a characteristic scale of the velocity, and $Re_M = Pr_M Re$. In this paper, we take this path and lower Pr_M significantly using high-resolution simulations.
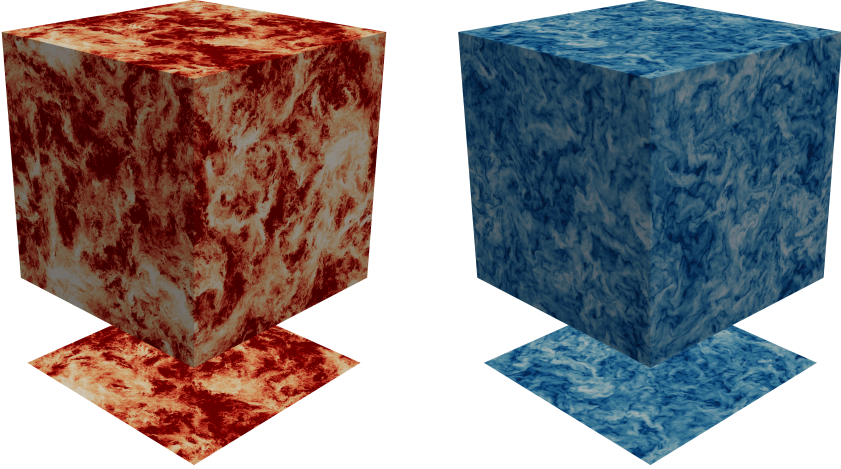
Fig. 1 **Visualisation of flow and SSD solution.** Flow speed (left) and magnetic field strength (right) from a high resolution SSD-active run with Re = 18200 and $Pr_M = 0.01$ on the surface of the simulation box.
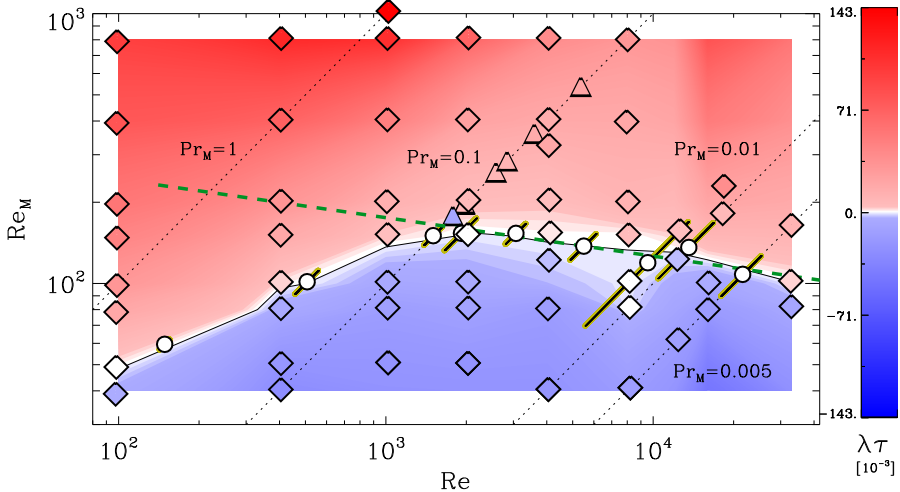
Results

We include simulations with resolutions of 256^3 to 4608^3 grid points and Re = 46 to 33000. This allows us to explore the parameter space from $Pr_M = 1$ to 0.0025, which is closer to the solar value than has been investigated in previous studies. For each run, we measure the growth rate λ of the magnetic field in its kinematic stage and determine whether or not an SSD is being excited.

To afford an in-depth exploration of the effect of Pr_M, we omit large-scale effects such as stratification, rotation and shear. We avoid the excessive integration times, required to simulate convection, by driving the turbulent flow explicitly under isothermal conditions. Our simulation setup consists of a fully periodic box with a random volume force, see Online Methods for details; the flow exhibits a Mach number of around 0.08. In Fig. 1, we visualize the velocity and magnetic fields of one of the highest resolution and Reynolds number cases. As might be anticipated for low Pr_M turbulence, the flow exhibits much finer, fractal-like structures than the magnetic field. Note, that all our results refer to the kinematic stage of the SSD, where the magnetic field strength is far too weak to influence the flow and otherwise arbitrary.

Growth rates and critical magnetic Reynolds numbers

In Fig. 2 we visualize the growth rate λ as function of Re and Re_M. We find positive growth rates for all sets of runs with constant Pr_M if Re_M is large enough. λ increases always with increasing Re_M as expected. Surprisingly, the growth rates are significantly lower within the interval from Re = 2000 to

Fig. 2   Small-scale dynamo growth rate as function of the fluid and magnetic Reynolds numbers (Re **and** $\mathrm{Re_M}$**).** The diamonds represent the results of this work and the triangles those of [10]. The color coding indicates the value of the normalized growth rate $\lambda\tau$ with $\tau = 1/u_{\mathrm{rms}}k_{\mathrm{f}}$, a rough estimate for the turnover time. Dotted lines indicate constant magnetic Prandtl number $\mathrm{Pr_M}$. White circles indicate zero growth rate for certain $\mathrm{Pr_M}$, obtained from fitting for the critical magnetic Reynolds number, as shown in Fig. 3; fitting errors are signified by yellow-black bars. see Supplementary Material, Section 5. The background colors including the thin black line (zero growth) are assigned via linear interpolation of the simulation data. The green dashed line shows the power-law fit of the critical $\mathrm{Re_M}$ for $\mathrm{Pr_M} \leq 0.08$, with power 0.125, see Fig. 3b.

10000 than below and above. With the $\mathrm{Re_M}$ values used, this maps roughly to a $\mathrm{Pr_M}$ interval from about 0.1 to 0.04.

The growth rates for $\mathrm{Pr_M} = 0.1$ match very well the ones from [10], indicated by triangles. From Fig. 2, we clearly see that the critical magnetic Reynolds number $\mathrm{Re_M^{crit}}$, defined by growth rate $\lambda = 0$, first rises as a function of Re and then falls for $\mathrm{Re} > 3 \times 10^3$, see the thin black line. Looking at $\mathrm{Re_M^{crit}}$ as a function of magnetic Prandtl number $\mathrm{Pr_M}$, it first increases with decreasing $\mathrm{Pr_M}$ and then decreases for $\mathrm{Pr_M} < 0.05$. Hence, an SSD is easier to excite here than for $0.05 < \mathrm{Pr_M} < 0.1$. We could even find a nearly marginal, positive growth rate for $\mathrm{Pr_M} = 0.003125$. The decrease of λ at low $\mathrm{Pr_M}$ is an important result as the SSD was believed to be even harder [4, 9] or at least equally hard [7, 8] to excite when $\mathrm{Pr_M}$ was decreased further from previously investigated values. The growth rates agree qualitatively with the earlier work at low $\mathrm{Pr_M}$ [6–8].

For a more accurate determination of $\mathrm{Re_M^{crit}}$, we next plot the growth rates for fixed $\mathrm{Pr_M}$ as a function of $\mathrm{Re_M}$, see Fig. 3(a). The data are consistent with $\lambda \propto \ln(\mathrm{Re_M}/\mathrm{Re_M^{crit}})$ as theoretically predicted [36, 37]. Fitting accordingly, we are able to determine $\mathrm{Re_M^{crit}}$ as a function of $\mathrm{Pr_M}$, see Fig. 3(b). The latter plot clearly shows that there are three distinct regions of dynamo excitation: When $\mathrm{Pr_M}$ decreases in the range $1 \geq \mathrm{Pr_M} \geq 0.1$ it becomes much harder to excite
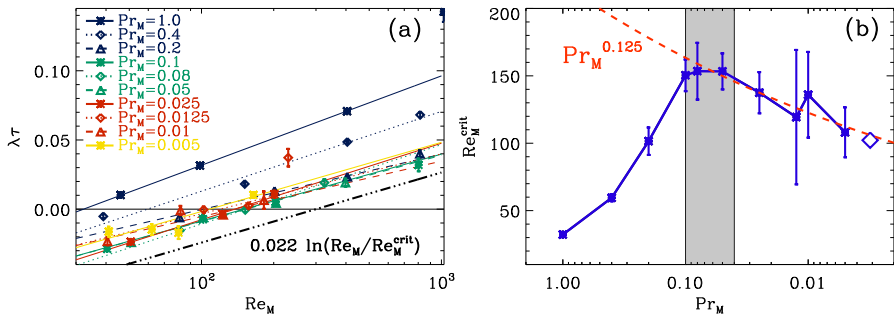
Fig. 3 Growth rate and critical Reynolds number. Panel (a): normalized growth rate $\lambda\tau$ as function of magnetic Reynolds number $\mathrm{Re_M}$ for simulation sets with fixed magnetic Prandtl number $\mathrm{Pr_M}$, indicated by different colors. Logarithmic functions $\lambda\tau \propto \ln(\mathrm{Re_M}/\mathrm{Re_M^{crit}})$ according to [36, 37] were fitted separately to the individual sets, as indicated by the colored lines; see the dashed-dotted line for the mean slope. Panel (b): critical magnetic Reynolds number $\mathrm{Re_M^{crit}}$ as function of $\mathrm{Pr_M}$ obtained from the fits in panel (a). Error bars show the fitting error, see Supplementary Material, Section 5. The diamond indicates a run with growth rate $\lambda \approx 0$, hence its $\mathrm{Re_M}$ represents $\approx \mathrm{Re_M^{crit}}$ for the used $\mathrm{Pr_M} = 0.003125$. The red dashed line is a power law fit $\mathrm{Re_M^{crit}} \propto \mathrm{Pr_M^{0.125}}$, valid for $\mathrm{Pr_M} \lesssim 0.08$. The grey shaded area indicates the $\mathrm{Pr_M}$ interval where the dynamo is hardest to excite ($\mathrm{Re_M^{crit}} \gtrsim 150$).

the SSD. In the range $0.1 \geq \mathrm{Pr_M} \geq 0.04$, excitation is most difficult with little variation of $\mathrm{Re_M^{crit}}$. For $\mathrm{Pr_M} \leq 0.04$, it again becomes easier as $\mathrm{Pr_M}$ reduces. In [7, 8], the authors already found an indication of $\mathrm{Re_M^{crit}}$ to level-off with decreasing $\mathrm{Pr_M}$, however only when using artificial hyperdiffusion. Similarly, with our error bars, a constant $\mathrm{Re_M^{crit}}$ cannot be excluded for $0.01 < \mathrm{Pr_M} < 0.1$. However, at $\mathrm{Pr_M} = 0.005$, the error bar allows to conclude that $\mathrm{Re_M^{crit}}$ is here lower than at $\mathrm{Pr_M} = 0.05$. This again confirms our result that $\mathrm{Re_M^{crit}}$ is decreasing with $\mathrm{Pr_M}$ for very low $\mathrm{Pr_M}$.

For $\mathrm{Pr_M} \leq 0.05$, the decrease of $\mathrm{Re_M^{crit}}$ with $\mathrm{Pr_M}$ can be well represented by the power-law $\mathrm{Re_M^{crit}} \propto \mathrm{Pr_M^{0.125}}$. Extrapolating this to the Sun and solar-like stars would lead to $\mathrm{Re_M^{crit}} \approx 40$ at $\mathrm{Pr_M} = 10^{-6}$, which means that we could expect an SSD to be present. For increasing Re, by decreasing ν, it would be reasonable to assert that the statistical properties of the flow and hence $\mathrm{Re_M^{crit}}$ become independent of $\mathrm{Pr_M}$. However, episodes of non-monotonic behavior of $\mathrm{Re_M^{crit}}$ when approaching this limit cannot be ruled out.

The well-determined $\mathrm{Re_M^{crit}}$ dependency on $\mathrm{Pr_M}$ together with its error bars and the power-law fit have been added to Fig. 2, and agree very well with the thin black line for $\lambda = 0$ interpolated from the growth rates.

Regions of dynamo excitation

Next we seek answers to the obvious question arising: why is the SSD harder to excite in a certain intermediate range of $\mathrm{Pr_M}$ and easier at lower and higher values? For this, we investigate the kinetic and magnetic energy spectra of a representative subset of the runs, see Supplementary Table 2. We show in Fig. 4 spectra of two exemplary cases: Run F005, with $\mathrm{Pr_M} = 0.05$, probes the
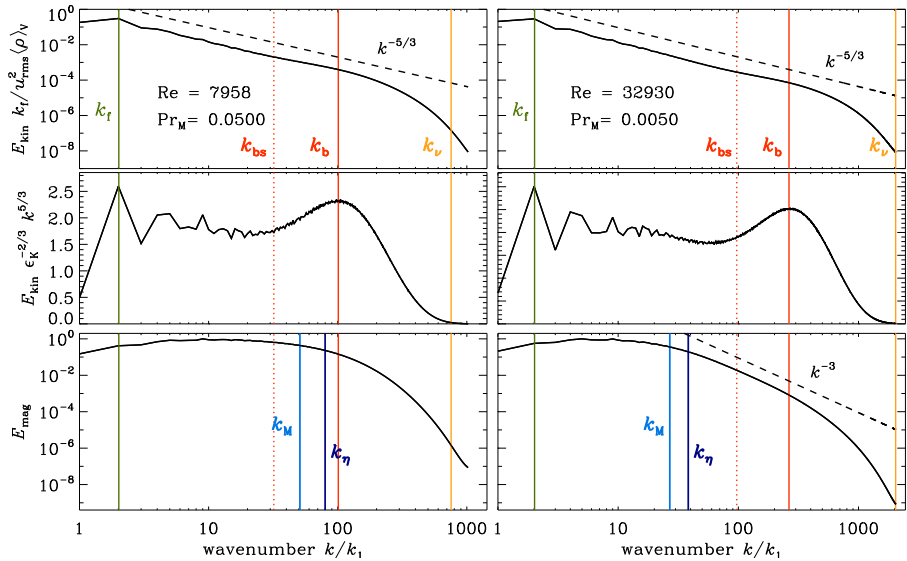
Fig. 4 Energy spectra. Kinetic (top row) and magnetic (bottom row) energy spectra for two exemplary runs with Re = 7958, $Pr_M = 0.05$ (left column) and Re = 32930, $Pr_M = 0.005$ (right column). In the middle row, the kinetic spectra are compensated by $k^{5/3}$. Vertical lines indicate the forcing wavenumber k_f (green solid), the wavenumber of the bottleneck's peak k_b (red solid) and its starting point k_{bs} (red dotted), the viscous dissipation wavenumber k_ν (orange), the ohmic dissipation wavenumber $k_\eta = k_\nu Pr_M^{3/4}$ (dark blue) and the characteristic magnetic wavenumber k_M (light blue). All spectra are averaged over the kinematic phase whereupon each individual magnetic spectrum was normalized by its maximum, thus taking out the exponential growth.

Pr_M interval of impeded dynamo action, while Run H0005, with $Pr_M = 0.005$, is clearly outside it; see Supplementary Fig. 1 and 2 for spectra of other cases.

In all cases the kinetic energy clearly follows a Kolmogorov cascade with $E_{kin} \propto k^{-5/3}$ in the inertial range. When compensating with $k^{5/3}$, we find the well-known bottleneck effect [38, 39]: a local increase in spectral energy, deviating from the power-law, as found both in fluid experiments [40–42] and numerical studies [43, 44]. It has been postulated to be detrimental to SSD growth [4, 10]. For the magnetic spectrum on the other hand, yet clearly visible only for $Pr_M \leq 0.005$, we find a power-law following $E_{mag} \propto k^{-3}$. A 3/2 slope at low wavenumbers as predicted by [45] is seen only in the runs with Pr_M close to one, while for the intermediate and low Pr_M runs, the positive-slope part of the spectrum shrinks to cover only the lowest k values, and the steep negative slopes at high k values become prominent. A steep negative slope in the magnetic power spectra was also seen by [7] for Pr_M slightly below unity. However, the authors propose a tentative power of -1 given that the -3 slope is not yet clearly visible for their Pr_M values.

Analyzing our simulations, we adopt the following strategy: For each spectrum, we determine the wavenumber of the bottleneck, k_b, as the location of its maximum in the (smoothed) compensated spectrum, along with its starting
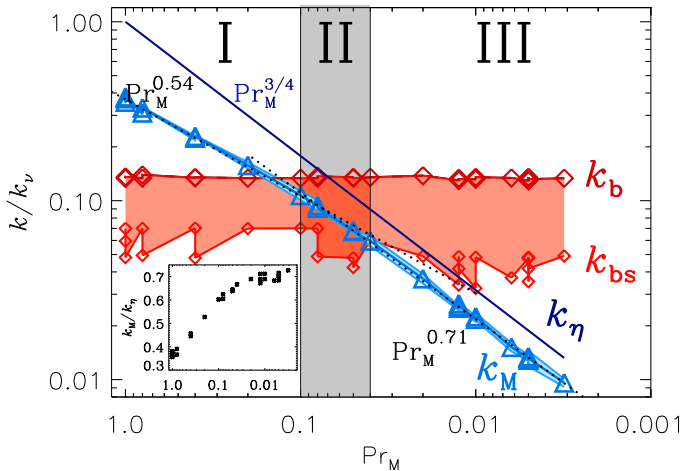
Fig. 5 Relation of the characteristic magnetic wavenumber k_M to the bottleneck. We show its peak k_b and its starting point k_{bs} in red, the characteristic magnetic wavenumber k_M in light blue and the ohmic dissipation wavenumber k_η in dark blue. The red shaded area between k_b and k_{bs} corresponds to the low-wavenumber part of the bottleneck where the turbulent flow is rougher than for a $-5/3$ power-law. The Roman numbers indicate the three distinct regions of dynamo excitation. The region of the weakest growth (II) is over-plotted in grey. The characteristic magnetic wavenumber k_M can be fitted by two power laws (black dotted lines): $k_M/k_\nu \propto \mathrm{Pr}_M^{0.54}$ for $\mathrm{Pr}_M \geq 0.05$ and $k_M/k_\nu \propto \mathrm{Pr}_M^{0.71}$ for $\mathrm{Pr}_M \leq 0.05$. All wavenumbers are normalized by the viscous one k_ν. We find that the dynamo is hardest to excite if k_M lies within the low-wavenumber side of the bottleneck. Leaving this region towards lower or higher wavenumbers makes the dynamo easier to excite. The inset shows k_M/k_η as a function of Pr_M.

point $k_{bs} < k_b$ at the location with 75% of the maximum, see the middle-row panels of Fig. 4. We additionally calculate a characteristic magnetic wavenumber, defined as $k_M = \int_k E_{\mathrm{mag}}(k)k\,dk / \int_k E_{\mathrm{mag}}(k)\,dk$, which is often connected with the energy-carrying scale. Furthermore, we calculate the viscous dissipation wavenumber $k_\nu = (\epsilon_K/\nu^3)^{1/4}$ following Kolmogorov theory, where ϵ_K is the viscous dissipation rate $2\nu\mathsf{S}^2$ with the traceless rate-of-strain tensor of the flow, S. From the relations between these four wavenumbers (listed in Supplementary Table 2), we will draw insights about the observed behavior of $\mathrm{Re}_M^{\mathrm{crit}}$ with respect to Pr_M.

We plot k_b/k_ν and k_{bs}/k_ν as functions of Pr_M in Fig. 5. As is expected, k_b/k_ν, or the ratio of the viscous scale to the scale of the bottleneck, does not depend on Pr_M, as the bottleneck is a purely hydrodynamic phenomenon. The start of the bottleneck k_{bs} should likewise not depend on Pr_M, but the low Re values for $\mathrm{Pr}_M = 1$ to 0.1 lead to apparent thinner bottlenecks, hence an unsystematic weak dependency. The red shaded area between k_b and k_{bs} is the low-wavenumber part of bottleneck where the slope of the spectrum is larger (less negative) than $-5/3$ see Supplementary Table 2 for values of the modified slope α_b and Supplementary, Section 1 for a discussion. We note that $\alpha_b \approx -1.3 \ldots -1.5$ and can thus deviate significantly from $-5/3$. Overplotting the k_M/k_ν curve reveals that it intersects with the red shaded area exactly

where the dynamo is hardest to excite (region II). This lets us conclude that the shallower slope of the low-wavenumber part of the bottleneck may indeed be responsible for enhancing $\mathrm{Re}_\mathrm{M}^\mathrm{crit}$ in the interval $0.04 \leq \mathrm{Pr}_\mathrm{M} \leq 0.1$. Using this plot, we can now clearly explain the three regions of dynamo excitation. For $0.1 \leq \mathrm{Pr}_\mathrm{M} \leq 1$ the low-wavenumber part of bottleneck and the characteristic magnetic scale are completely decoupled. This makes the SSD easy to excite (region I). For $0.04 \leq \mathrm{Pr}_\mathrm{M} \leq 0.1$, (grey, region II), the dynamo is hardest to excite because of the shallower slope of the kinetic spectra. In region III, where $\mathrm{Pr}_\mathrm{M} \leq 0.04$ the low-wavenumber part of bottleneck and the characteristic magnetic scale are again completely decoupled making the dynamo easier to excite.

Further, we find that the dependence of k_M/k_ν on Pr_M also differs between the regions. In region I k_M/k_ν depends on Pr_M via $k_\mathrm{M}/k_\nu \propto \mathrm{Pr}_\mathrm{M}^{0.54}$ and in region II and III via $k_\mathrm{M}/k_\nu \propto \mathrm{Pr}_\mathrm{M}^{0.71}$. This becomes particularly interesting when comparing the characteristic magnetic wavenumber k_M with the ohmic dissipation wavenumber which is defined as $k_\eta = k_\nu \mathrm{Pr}_\mathrm{M}^{3/4}$. In region I, we find a significant difference of k_M and k_η in value and scaling. However, in region III the scaling of k_M comes very close to the $3/4$ scaling of k_η. This behaviour can be even better seen in the inset of Fig. 5, where the ratio k_M/k_η is 0.3 for $\mathrm{Pr}_\mathrm{M} = 1$ and tends towards unity for decreasing Pr_M, but is likely to saturate below 0.75.

Discussion

In conclusion, we find that the SSD is progressively easier to excite for magnetic Prandtl numbers below 0.04, in contrast to earlier findings, and thus is very likely to exist in the Sun and other cool stars. Provided saturation at sufficiently high levels, the SSD has been proposed to strongly influence the dynamics of solar-like stars: previous numerical studies, albeit at $\mathrm{Pr}_\mathrm{M} \approx 1$, indicate that this influence concerns for example the angular momentum transport [19, 20], and the LSD [21–25]. Our kinematic study, however, only shows that a positive growth rate is possible at very low Pr_M, but not whether an SSD is able to generate dynamically important field strengths. As the Re_M of the Sun and solar-like stars is several orders of magnitude higher than the extrapolated $\mathrm{Re}_\mathrm{M}^\mathrm{crit}$ value of 40, we yet expect dynamically important SSDs as indicated by $\mathrm{Pr}_\mathrm{M} = 1$ simulations [15]. However, numerical simulations with Pr_M down to 0.01 show a decrease of the saturation strength with decreasing Pr_M [46].

The results of our study are well in agreement with previous numerical studies considering partly overlapping Pr_M ranges [6–8, 10]. Those found some discrepancies with the Kazantsev theory [45] for low Pr_M, for example the narrowing down of the positive Kazantsev spectrum at low and intermediate wavenumbers, and the emergence of a negative slope instead at large wave numbers [7]. We could extend this regime to even lower Pr_M and therefore study these discrepancies further. For $\mathrm{Pr}_\mathrm{M} \leq 0.005$ we find that the magnetic

spectrum shows a power-law scaling k^{-3}, which is significantly steeper than the tentative k^{-1} one proposed in [7] for $0.03 \lesssim \mathrm{Pr_M} \lesssim 0.07$ (but only for 8th-order hyperdiffusivity). This latest finding of such a steep power law in the magnetic spectrum challenges the current theoretical predictions and might indicate that the SSD operating at low $\mathrm{Pr_M}$ is fundamentally different from that at $\mathrm{Pr_M} \approx 1$.

Secondly, we find that the growth rates near the onset follow an $\ln(\mathrm{Re_M})$ dependence as predicted by [36, 37], and not a $\mathrm{Re_M^{1/2}}$ one as would result from intertial-range-driven SSD [1, 7]. We do not observe a tendency of the growth rate to become independent of $\mathrm{Re_M}$ at the highest $\mathrm{Pr_M}$ either, which could be an indication of an outer-scale driven SSD, as postulated by [7]. Furthermore, we find that the pre-factor of $\gamma \propto \ln(\mathrm{Re_M}/\mathrm{Re_M^{crit}})$ is nearly constant with its mean around 0.022, in agreement with 0.023 of [10]. A constant value means that the logarithmic scaling is independent of $\mathrm{Pr_M}$ and seems to be of general validity.

Thirdly, we find that the measured characteristic magnetic wavenumber k_M is always smaller than the estimated k_η, and furthermore, k_M is not always following the theory-predicted scaling of $k_\eta \propto \mathrm{Pr_M^{3/4}}$ with $\mathrm{Pr_M}$. For the region I, where $\mathrm{Pr_M}$ is close to 1, this discrepancy is up to a factor of three and the deviation from the expected $\mathrm{Pr_M}$-scaling is most significant here. These discrepancies have been associated with the numerical setups injecting energy at a forcing scale far larger than the dissipation scale, i.e. $k_f \ll k_\eta$ [1]. Furthermore, our runs in region I also have relatively low Re and therefore numerical effects are not dismissible. In region III (low $\mathrm{Pr_M}$), k_M/k_η is approaching the constant offset factor 0.75. Hence, the scaling of k_M/k_ν with $\mathrm{Pr_M}$ gets close to the expected one. This result again indicates that the SSD at low $\mathrm{Pr_M}$ is different from that at $\mathrm{Pr_M} \approx 1$.

An increase of $\mathrm{Re_M^{crit}}$ with decreasing $\mathrm{Pr_M}$ followed by an asymptotic levelling-off for $\mathrm{Pr_M} \ll 1$ was expected in the light of theory and previous numerical studies. Instead, we found non-monotonic behavior as function of $\mathrm{Pr_M}$; we could relate it to the hydrodynamical phenomenon of the bottleneck. If the characteristic magnetic wavenumber lies in the positive-gradient part of the compensated spectrum, where the spectral slope is significantly reduced from $-5/3$ to ~ -1.4, the dynamo is hardest to excite ($0.1 \geq \mathrm{Pr_M} \geq 0.04$). For higher or lower $\mathrm{Pr_M}$, the dynamo becomes increasingly easier to excite. The local change in slope due to the bottleneck has often been related to an increase of the "roughness" of the flow [1, 10, 43], which is expected to harden dynamo excitation based on theoretical predictions [4, 9] from kinematic Kazantsev theory [45]. In line with theory, the roughness-increasing part of the bottleneck appears decisive in our results, however, only when k_M is used as a criterion. The usage of k_η would in contrast suggest that the peak of the bottleneck is decisive [10]. Such interpretation appears incorrect, as the rough estimate of k_η employed here does not represent the magnetic spectrum adequately and the peak of the bottleneck does not coincide with the maximum of "roughness".

Online Methods

Numerical setup

For our simulations, we use a cubic Cartesian box with edge length L and solve the isothermal magnetohydrodynamic equations without gravity, similar as in [5, 47].

$$\frac{\mathrm{D}\boldsymbol{u}}{\mathrm{D}t} = -c_\mathrm{s}^2 \boldsymbol{\nabla} \ln \rho + \boldsymbol{J} \times \boldsymbol{B}/\rho + \boldsymbol{\nabla} \cdot (2\rho\nu\mathbf{S})/\rho + \boldsymbol{f}, \tag{1}$$

$$\frac{\partial \boldsymbol{A}}{\partial t} = \boldsymbol{u} \times \boldsymbol{B} + \eta\boldsymbol{\nabla}^2\boldsymbol{A}, \tag{2}$$

$$\frac{\mathrm{D}\rho}{\mathrm{D}t} = -\boldsymbol{\nabla} \cdot (\rho\boldsymbol{u}), \tag{3}$$

where $\boldsymbol{u}$ is the flow speed, c_s is the sound speed, ρ is the mass density, and $\boldsymbol{B} = \boldsymbol{\nabla} \times \boldsymbol{A}$ is the magnetic field with $\boldsymbol{A}$ being the vector potential. $\boldsymbol{J} = \boldsymbol{\nabla} \times \boldsymbol{B}/\mu_0$ is the current density with magnetic vacuum permeability μ_0, while ν and η are constant kinematic viscosity and magnetic diffusivity, respectively. The rate-of-strain tensor $\mathbf{S}_{ij} = (u_{i,j} + u_{j,i})/2 - \delta_{ij}\boldsymbol{\nabla} \cdot \boldsymbol{u}/3$ is traceless. The forcing function $\boldsymbol{f}$ provides random white-in-time non-helical transversal plane waves, which are added in each time step to the momentum equation, see [5] for details. The wavenumbers of the forcing lie in a narrow band around $k_\mathrm{f} = 2k_1$ with $k_1 = 2\pi/L$. Its amplitude is chosen such that the Mach number $\mathrm{Ma} = u_\mathrm{rms}/c_\mathrm{s}$ is always around 0.082, where $u_\mathrm{rms} = \sqrt{\langle \boldsymbol{u}^2 \rangle_V}$ is the volume and time-averaged root-mean-square value. The Ma values of all runs are listed in Supplementary Material Table 1. To normalize the growth rate λ, we use an estimated turnover time $\tau = 1/u_\mathrm{rms}k_\mathrm{f} \approx 6/k_1c_\mathrm{s}$. The boundary conditions are periodic for all quantities and we initialise the magnetic field with weak Gaussian noise.

Diffusion is controlled by the prescribed parameters ν and η. Accordingly, we define the fluid and magnetic Reynolds numbers with the forcing wavenumber k_f as

$$\mathrm{Re} = u_\mathrm{rms}/\nu k_\mathrm{f}, \quad \mathrm{Re_M} = u_\mathrm{rms}/\eta k_\mathrm{f}. \tag{4}$$

We performed numerical free decay experiments (see Supplementary Material, Section 7), from which we confirm that the numerical diffusivities are negligible.

The spectral kinetic and magnetic energy densities are defined via

$$\int_k E_\mathrm{kin}(k)\, dk = u_\mathrm{rms}^2 \langle \rho \rangle_V / 2, \tag{5}$$

$$\int_k E_\mathrm{mag}(k)\, dk = B_\mathrm{rms}^2 / 2\mu_0, \tag{6}$$

where $B_{\mathrm{rms}} = \sqrt{\langle \boldsymbol{B}^2 \rangle_V}$ is the volume-averaged root-mean-square value and $\langle \rho \rangle_V$ the volume-averaged density.

Our numerical setup employs a drastically simplified model of turbulence compared to the actual one in the Sun. There, turbulence is driven by stratified rotating convection being of course neither isothermal nor isotropic. However, these simplifications were to date necessary when performing a parameter study at such high resolutions as we do. Nevertheless, we can connect our study to solar parameters in terms of $\mathrm{Pr_M}$ and Ma. Their chosen values best represent the weakly stratified layers within the bulk of the solar convection zone, where $\mathrm{Pr_M} \ll 1$ and $\mathrm{Ma} \ll 1$. The anisotropy in the flow on small scales is much weaker there than near the surface and therefore close to our simplified setup.

Data availability

Data for reproducing Figs. 2, 3, and 5 are included in the article and its supplementary information files. The raw data (time-series, spectra, slices, and snapshots) are provided through IDA/Fairdata service hosted at CSC, Finland, under https://doi.org/10.23729/206af669-07fd-4a30-9968-b4ded5003014. From the raw data, Figs. 1 and 4 can be reproduced.

Code availability

We use the Pencil Code [48] to perform all simulations, with parallelized fast-Fourier-transforms to calculate the spectra on the fly [49]. Pencil Code is freely available under https://github.com/pencil-code/.

Acknowledgements

Author Contributions Statement

JW was leading, but all the authors contributed, to the design and performing the numerical simulations. JW was leading the data analysis. MJKL was in charge of acquiring the computational resources from CSC. All the authors contributed to the interpretation of the results and writing up the manuscript.

Competing Interests Statement

The authors declare no competing interests.

References

[1] Brandenburg, A., Subramanian, K.: Astrophysical magnetic fields and nonlinear dynamo theory. Phys. Rep. **417**, 1–209 (2005) https://arxiv.org/abs/arXiv:astro-ph/0405052. https://doi.org/10.1016/j.physrep.2005.06.005

[2] Charbonneau, P.: Dynamo models of the solar cycle. Living Reviews in Solar Physics **17**(1), 4 (2020). https://doi.org/10.1007/s41116-020-00025-6

[3] Childress, S., Gilbert, A.D.: Stretch, twist, fold: The fast dynamo. Lecture Notes in Physics Monographs **37** (1995)

[4] Boldyrev, S., Cattaneo, F.: Magnetic-Field Generation in Kolmogorov Turbulence. Phys. Rev. Lett. **92**(14), 144501 (2004) https://arxiv.org/abs/astro-ph/0310780 [astro-ph]. https://doi.org/10.1103/PhysRevLett.92.144501

[5] Haugen, N.E.L., Brandenburg, A.: Suppression of small scale dynamo action by an imposed magnetic field. Phys. Rev. E **70**(3), 036408 (2004) https://arxiv.org/abs/arXiv:astro-ph/0402281. https://doi.org/10.1103/PhysRevE.70.036408

[6] Schekochihin, A.A., Cowley, S.C., Maron, J.L., McWilliams, J.C.: Critical Magnetic Prandtl Number for Small-Scale Dynamo. Phys. Rev. Lett. **92**(5), 054502 (2004) https://arxiv.org/abs/astro-ph/0308336 [astro-ph]. https://doi.org/10.1103/PhysRevLett.92.054502

[7] Schekochihin, A.A., Iskakov, A.B., Cowley, S.C., McWilliams, J.C., Proctor, M.R.E., Yousef, T.A.: Fluctuation dynamo and turbulent induction at low magnetic Prandtl numbers. New Journal of Physics **9**(8), 300 (2007) https://arxiv.org/abs/0704.2002 [physics.flu-dyn]. https://doi.org/10.1088/1367-2630/9/8/300

[8] Iskakov, A.B., Schekochihin, A.A., Cowley, S.C., McWilliams, J.C., Proctor, M.R.E.: Numerical Demonstration of Fluctuation Dynamo at Low Magnetic Prandtl Numbers. Phys. Rev. Lett. **98**(20), 208501 (2007) https://arxiv.org/abs/astro-ph/0702291 [astro-ph]. https://doi.org/10.1103/PhysRevLett.98.208501

[9] Schober, J., Schleicher, D., Bovino, S., Klessen, R.S.: Small-scale dynamo at low magnetic Prandtl numbers. Phys. Rev. E **86**(6), 066412 (2012)

https://arxiv.org/abs/1212.5979 [astro-ph.CO]. https://doi.org/10.1103/PhysRevE.86.066412

[10] Brandenburg, A., Haugen, N.E.L., Li, X.-Y., Subramanian, K.: Varying the forcing scale in low Prandtl number dynamos. MNRAS **479**(2), 2827–2833 (2018) https://arxiv.org/abs/1805.01249 [physics.flu-dyn]. https://doi.org/10.1093/mnras/sty1570

[11] Stix, M.: The Sun: an Introduction. Springer, Berlin (2002)

[12] Cattaneo, F.: On the Origin of Magnetic Fields in the Quiet Photosphere. ApJ **515**(1), 39–42 (1999). https://doi.org/10.1086/311962

[13] Vögler, A., Schüssler, M.: A solar surface dynamo. A&A **465**(3), 43–46 (2007) https://arxiv.org/abs/astro-ph/0702681 [astro-ph]. https://doi.org/10.1051/0004-6361:20077253

[14] Kitiashvili, I.N., Kosovichev, A.G., Mansour, N.N., Wray, A.A.: Realistic Modeling of Local Dynamo Processes on the Sun. ApJ **809**(1), 84 (2015) https://arxiv.org/abs/1506.08924 [astro-ph.SR]. https://doi.org/10.1088/0004-637X/809/1/84

[15] Hotta, H., Rempel, M., Yokoyama, T.: Efficient Small-scale Dynamo in the Solar Convection Zone. ApJ **803**(1), 42 (2015) https://arxiv.org/abs/1502.03846 [astro-ph.SR]. https://doi.org/10.1088/0004-637X/803/1/42

[16] Rempel, M.: Numerical Simulations of Quiet Sun Magnetism: On the Contribution from a Small-scale Dynamo. ApJ **789**, 132 (2014) https://arxiv.org/abs/1405.6814 [astro-ph.SR]. https://doi.org/10.1088/0004-637X/789/2/132

[17] Rempel, M.: Small-scale Dynamo Simulations: Magnetic Field Amplification in Exploding Granules and the Role of Deep and Shallow Recirculation. ApJ **859**(2), 161 (2018) https://arxiv.org/abs/1805.08390 [astro-ph.SR]. https://doi.org/10.3847/1538-4357/aabba0

[18] Riva, F., Steiner, O.: Methodology for estimating the magnetic Prandtl number and application to solar surface small-scale dynamo simulations. A&A **660**, 115 (2022) https://arxiv.org/abs/2202.12115 [astro-ph.SR]. https://doi.org/10.1051/0004-6361/202142644

[19] Käpylä, P.J., Käpylä, M.J., Olspert, N., Warnecke, J., Brandenburg, A.: Convection-driven spherical shell dynamos at varying Prandtl numbers. A&A **599**, 4 (2017) https://arxiv.org/abs/1605.05885 [astro-ph.SR]. https://doi.org/10.1051/0004-6361/201628973

[20] Hotta, H., Kusano, K.: Solar differential rotation reproduced

with high-resolution simulation. Nature Astronomy **5**, 1100–1102 (2021) https://arxiv.org/abs/2109.06280 [astro-ph.SR]. https://doi.org/10.1038/s41550-021-01459-0

[21] Tobias, S.M., Cattaneo, F.: Shear-driven dynamo waves at high magnetic Reynolds number. Nature **497**(7450), 463–465 (2013). https://doi.org/10.1038/nature12177

[22] Bhat, P., Subramanian, K., Brandenburg, A.: A unified large/small-scale dynamo in helical turbulence. MNRAS **461**(1), 240–247 (2016) https://arxiv.org/abs/1508.02706 [astro-ph.GA]. https://doi.org/10.1093/mnras/stw1257

[23] Squire, J., Bhattacharjee, A.: The magnetic shear-current effect: generation of large-scale magnetic fields by the small-scale dynamo. Journal of Plasma Physics **82**(2), 535820201 (2016) https://arxiv.org/abs/1512.04511 [astro-ph.HE]. https://doi.org/10.1017/S0022377816000258

[24] Hotta, H., Rempel, M., Yokoyama, T.: Large-scale magnetic fields at high reynolds numbers in magnetohydrodynamic simulations. Science **351**(6280), 1427–1430 (2016) https://arxiv.org/abs/http://science.sciencemag.org/content/351/6280/1427.full.pdf. https://doi.org/10.1126/science.aad1893

[25] Väisälä, M.S., Pekkilä, J., Käpylä, M.J., Rheinhardt, M., Shang, H., Krasnopolsky, R.: Interaction of Large- and Small-scale Dynamos in Isotropic Turbulent Flows from GPU-accelerated Simulations. ApJ **907**(2), 83 (2021) https://arxiv.org/abs/2012.08758 [physics.flu-dyn]. https://doi.org/10.3847/1538-4357/abceca

[26] Rempel, M.: Extension of the MURaM Radiative MHD Code for Coronal Simulations. ApJ **834**, 10 (2017) https://arxiv.org/abs/1609.09818 [astro-ph.SR]. https://doi.org/10.3847/1538-4357/834/1/10

[27] Kleint, L., Berdyugina, S.V., Shapiro, A.I., Bianda, M.: Solar turbulent magnetic fields: surprisingly homogeneous distribution during the solar minimum. A&A **524**, 37 (2010). https://doi.org/10.1051/0004-6361/201015285

[28] Buehler, D., Lagg, A., Solanki, S.K.: Quiet Sun magnetic fields observed by Hinode: Support for a local dynamo. A&A **555**, 33 (2013) https://arxiv.org/abs/1307.0789 [astro-ph.SR]. https://doi.org/10.1051/0004-6361/201321152

[29] Lites, B.W., Centeno, R., McIntosh, S.W.: The solar cycle dependence of the weak internetwork flux. PASJ **66**, 4 (2014). https://doi.org/10.1093/pasj/psu082

[30] Bellot Rubio, L., Orozco Suárez, D.: Quiet Sun magnetic fields: an observational view. Living Reviews in Solar Physics **16**(1), 1 (2019). https://doi.org/10.1007/s41116-018-0017-1

[31] Faurobert, M., Ricort, G.: Magnetic flux structuring of the quiet Sun internetwork. Center-to-limb analysis of solar-cycle variations. A&A **651**, 21 (2021) https://arxiv.org/abs/2105.08657 [astro-ph.SR]. https://doi.org/10.1051/0004-6361/202140705

[32] Korpi-Lagg, M.J., Korpi-Lagg, A., Olspert, N., Truong, H.-L.: Solar-Cycle Variation of quiet-Sun Magnetism and Surface Gravity Oscillation Mode. arXiv e-prints, 2205–04419 (2022) https://arxiv.org/abs/2205.04419 [astro-ph.SR]

[33] Tobias, S.M.: The turbulent dynamo. Journal of Fluid Mechanics **912**, 1 (2021) https://arxiv.org/abs/1907.03685 [physics.flu-dyn]. https://doi.org/10.1017/jfm.2020.1055

[34] Schekochihin, A.A., Haugen, N.E.L., Brandenburg, A., Cowley, S.C., Maron, J.L., McWilliams, J.C.: The Onset of a Small-Scale Turbulent Dynamo at Low Magnetic Prandtl Numbers. ApJ **625**(2), 115–118 (2005) https://arxiv.org/abs/astro-ph/0412594 [astro-ph]. https://doi.org/10.1086/431214

[35] Tobias, S.M., Cattaneo, F., Boldyrev, S.: In: Davidson, P.A., Kaneda, Y., Sreenivasan, K.R. (eds.) MHD Dynamos and Turbulence, pp. 351–404. Cambridge University Press, Cambridge, UK (2012). https://doi.org/10.1017/CBO9781139032810.010

[36] Rogachevskii, I., Kleeorin, N.: Intermittency and anomalous scaling for magnetic fluctuations. Phys. Rev. E **56**(1), 417–426 (1997). https://doi.org/10.1103/PhysRevE.56.417

[37] Kleeorin, N., Rogachevskii, I.: Growth rate of small-scale dynamo at low magnetic Prandtl numbers. Phys. Scr **86**(1), 018404 (2012) https://arxiv.org/abs/1112.3926 [astro-ph.SR]. https://doi.org/10.1088/0031-8949/86/01/018404

[38] Falkovich, G.: Bottleneck phenomenon in developed turbulence. Physics of Fluids **6**(4), 1411–1414 (1994). https://doi.org/10.1063/1.868255

[39] Lohse, D., Müller-Groeling, A.: Bottleneck Effects in Turbulence: Scaling Phenomena in r versus p Space. Phys. Rev. Lett. **74**(10), 1747–1750 (1995) https://arxiv.org/abs/chao-dyn/9405002 [nlin.CD]. https://doi.org/10.1103/PhysRevLett.74.1747

[40] She, Z.-S., Jackson, E.: On the universal form of energy spectra in fully

developed turbulence. Physics of Fluids A **5**(7), 1526–1528 (1993). https://doi.org/10.1063/1.858591

[41] Saddoughi, S.G., Veeravalli, S.V.: Local isotropy in turbulent boundary layers at high Reynolds number. Journal of Fluid Mechanics **268**, 333–372 (1994). https://doi.org/10.1017/S0022112094001370

[42] Küchler, C., Bewley, G., Bodenschatz, E.: Experimental Study of the Bottleneck in Fully Developed Turbulence. Journal of Statistical Physics **175**(3-4), 617–639 (2019) https://arxiv.org/abs/1812.01370 [physics.flu-dyn]. https://doi.org/10.1007/s10955-019-02251-1

[43] Dobler, W., Haugen, N.E., Yousef, T.A., Brandenburg, A.: Bottleneck effect in three-dimensional turbulence simulations. Phys. Rev. E **68**(2), 026304 (2003) https://arxiv.org/abs/astro-ph/0303324 [astro-ph]. https://doi.org/10.1103/PhysRevE.68.026304

[44] Donzis, D.A., Sreenivasan, K.R.: The bottleneck effect and the Kolmogorov constant in isotropic turbulence. Journal of Fluid Mechanics **657**, 171–188 (2010). https://doi.org/10.1017/S0022112010001400

[45] Kazantsev, A.P.: Enhancement of a Magnetic Field by a Conducting Fluid. Soviet Journal of Experimental and Theoretical Physics **26**, 1031 (1968)

[46] Brandenburg, A.: Nonlinear Small-scale Dynamos at Low Magnetic Prandtl Numbers. ApJ **741**(2), 92 (2011) https://arxiv.org/abs/1106.5777 [astro-ph.SR]. https://doi.org/10.1088/0004-637X/741/2/92

[47] Brandenburg, A.: The Inverse Cascade and Nonlinear Alpha-Effect in Simulations of Isotropic Helical Hydromagnetic Turbulence. ApJ **550**, 824–840 (2001) https://arxiv.org/abs/arXiv:astro-ph/0006186. https://doi.org/10.1086/319783

[48] Pencil Code Collaboration, Brandenburg, A., Johansen, A., Bourdin, P., Dobler, W., Lyra, W., Rheinhardt, M., Bingert, S., Haugen, N., Mee, A., Gent, F., Babkovskaia, N., Yang, C.-C., Heinemann, T., Dintrans, B., Mitra, D., Candelaresi, S., Warnecke, J., Käpylä, P., Schreiber, A., Chatterjee, P., Käpylä, M., Li, X.-Y., Krüger, J., Aarnes, J., Sarson, G., Oishi, J., Schober, J., Plasson, R., Sandin, C., Karchniwy, E., Rodrigues, L., Hubbard, A., Guerrero, G., Snodin, A., Losada, I., Pekkilä, J., Qian, C.: The Pencil Code, a modular MPI code for partial differential equations and particles: multipurpose and multiuser-maintained. JOSS **6**(58), 2807 (2021). https://doi.org/10.21105/joss.02807

[49] Bourdin, P.-A.: Driving solar coronal MHD simulations on high-performance computers. Geophysical and Astrophysical Fluid Dynamics **114**(1-2), 235–260 (2020) https://arxiv.org/abs/1908.08557 [astro-ph.SR]. https://doi.org/10.1080/03091929.2019.1643849

Numerical evidence for a small-scale dynamo approaching solar magnetic Prandtl numbers

Supplementary Material

Jörn Warnecke[1], Maarit J. Korpi-Lagg[2,1,3], Frederick A. Gent[2,4] and Matthias Rheinhardt[2]

[1] Max-Planck-Institut für Sonnensystemforschung, Justus-von-Liebig-Weg 3, D-37077 Göttingen, Germany
[2] Department of Computer Science, Aalto University, PO Box 15400, FI-00 076 Espoo, Finland
[3] Nordita, KTH Royal Institute of Technology & Stockholm University, Hannes Alfvéns väg 12, SE-11419, Sweden
[4] School of Mathematics, Statistics and Physics, Newcastle University, NE1 7RU, UK

March 13, 2023

1 Discussion on the roughness of the flow

We calculate the slope in the low-wavenumber part of the bottleneck by fitting $E_{\mathrm{mag}} \sim k^{\alpha_{\mathrm{b}}}$ in the interval $k_{\mathrm{bs}} \ldots k_{\mathrm{b}}$. As shown in Supplementary Fig. 1, the values of α_{b} are significantly different from $-5/3$ without the bottleneck. Furthermore, we find no clear systematic dependence of α_{b} on Re.
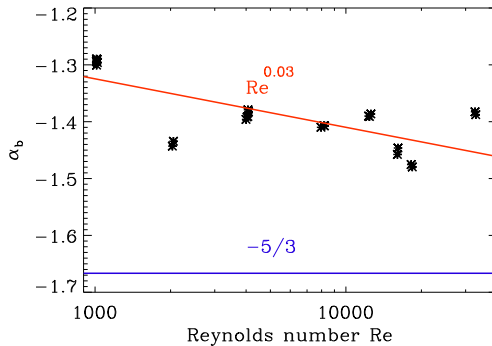
Supplementary Figure 1:   Slope of the low-wavenumber part of the bottleneck, α_{b}, as a function of fluid Reynolds number Re. The blue line indicates the slope $-5/3$ in the inertial range without bottleneck; the red line shows a power-law fit with $\mathrm{Re}^{0.03}$.

2 Spectra of a representative subset of the runs
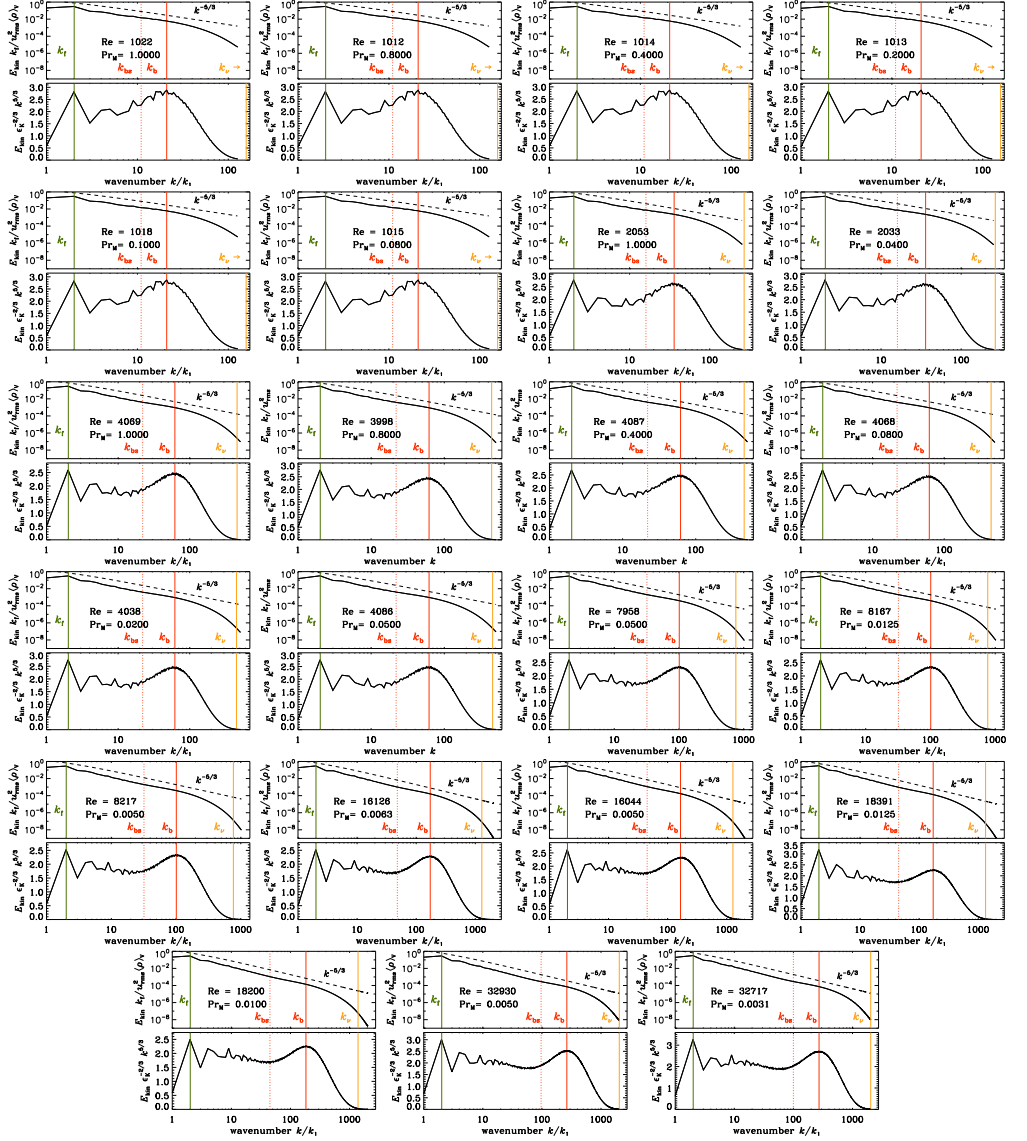
Supplementary Figure 2: Kinetic energy spectra, for explanations see Fig. 4. The notation "$k_\nu \to$" indicates that k_ν is outside the accessible k range.
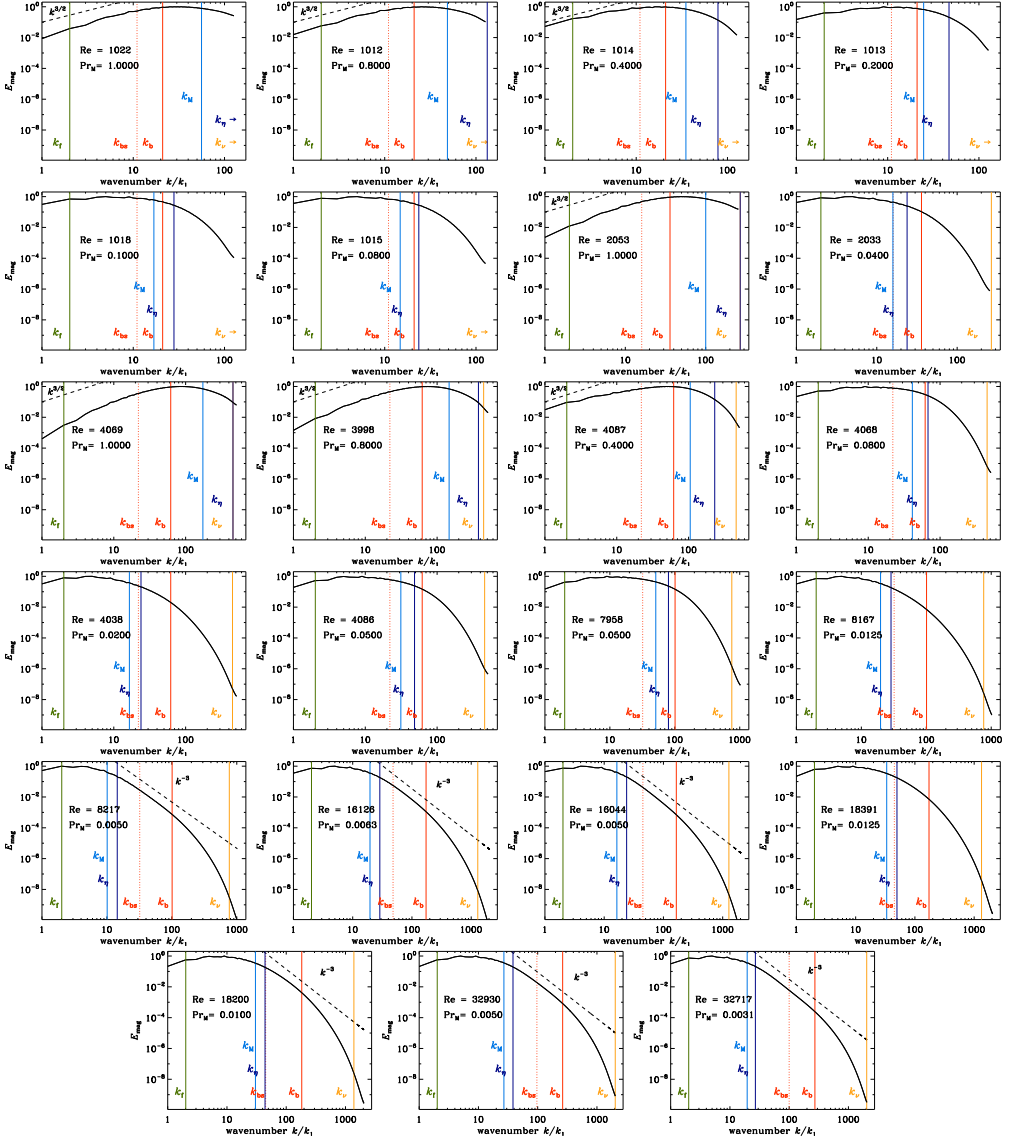
Supplementary Figure 3: Normalized magnetic energy spectra, for explanations see Fig 4. The notation "$k_{\nu,\eta} \rightarrow$" indicates that $k_{\nu,\eta}$ is outside the accessible k range.

3

3 Table of all runs

Supplementary Table 1: Overview of all performed runs.

Run	Resolution	$\mathrm{Pr_M}$	Re	$\mathrm{Re_M}$	Ma	$\lambda\tau$	$\sigma_\lambda\tau$
P10	256^3	1.00	46	46	0.075	0.0102	0.0015
A80	256^3	8.00	99	790	0.080	0.0962	0.0013
A40	256^3	4.00	99	394	0.080	0.0794	0.0016
A20	256^3	2.00	99	197	0.080	0.0557	0.0009
A15	256^3	1.50	99	148	0.080	0.0458	0.0010
A10	256^3	1.00	99	99	0.080	0.0315	0.0007
A08	256^3	0.80	98	78	0.079	0.0200	0.0008
A05	256^3	0.50	98	49	0.079	-0.0008	0.0019
A04	256^3	0.40	97	39	0.079	-0.0052	0.0016
B20	256^3	2.00	405	811	0.081	0.1129	0.0010
B10	256^3	1.00	404	404	0.081	0.0707	0.0004
B05	256^3	0.50	404	202	0.081	0.0334	0.0019
B0375	256^3	0.375	403	151	0.081	0.0182	0.0011
B025	256^3	0.25	405	101	0.081	0.0015	0.0010
B02	256^3	0.2	405	81	0.082	-0.0060	0.0025
B0125	256^3	0.125	405	51	0.082	-0.0217	0.0025
B01	256^3	0.1	404	40	0.082	-0.0287	0.0015
C10	256^3	1.00	1022	1022	0.082	0.1428	0.0075
C08	256^3	0.80	1014	811	0.082	0.1079	0.0028
C04	256^3	0.40	1013	405	0.082	0.0486	0.0007
C02	256^3	0.20	1008	201	0.081	0.0132	0.0009
C015	256^3	0.15	1014	152	0.082	0.0027	0.0008
C01	256^3	0.10	1013	101	0.081	-0.0074	0.0010
C008	256^3	0.08	1015	81	0.082	-0.0154	0.0022
C005	256^3	0.05	1019	51	0.082	-0.0239	0.0014
D10	512^3	1.00	2053	2053	0.083	0.1853	0.0052
D04	512^3	0.40	2038	815	0.082	0.0682	0.0017
D02	512^3	0.20	2026	405	0.082	0.0235	0.0006
D01	512^3	0.10	2038	204	0.082	0.0053	0.0021
D0075	512^3	0.075	2029	152	0.082	-0.0005	0.0015
D005	512^3	0.05	2031	102	0.082	-0.0058	0.0017
D004	512^3	0.04	2034	81	0.082	-0.0121	0.0009
D0025	512^3	0.025	2030	51	0.082	-0.0236	0.0017
E10	1024^3	1.00	4069	4069	0.082	0.2769	0.0126
E08	1024^3	0.80	3999	3199	0.081	0.2141	0.0091
E04	1024^3	0.40	4087	1635	0.082	0.1148	0.0324
E02	1024^3	0.20	4064	813	0.082	0.0401	0.0025
E01	1024^3	0.10	4075	407	0.082	0.0155	0.0009
E008	1024^3	0.08	4089	325	0.082	0.0191	0.0025
E005	1024^3	0.05	4090	205	0.082	0.0044	0.0021
E00375	1024^3	0.0375	4121	155	0.083	0.0006	0.0024
E003	1024^3	0.03	4084	123	0.082	-0.0035	0.0012
E002	1024^3	0.02	4037	81	0.081	-0.0163	0.0023
E001	1024^3	0.01	4043	40	0.082	-0.0232	0.0029

$\mathrm{Pr_M}$ is the magnetic Prandtl number, Re and $\mathrm{Re_M}$ are the fluid and magnetic Reynolds numbers, $\mathrm{Ma} = u_{\mathrm{rms}}/c_{\mathrm{s}}$ is the Mach number, $\tau = 1/u_{\mathrm{rms}}k_{\mathrm{f}}$ is a rough estimate for the turnover time, λ is the SSD growth rate with its error σ_λ.

Supplementary Table 1:   continued.

Run	Resolution	$\mathrm{Pr_M}$	Re	$\mathrm{Re_M}$	Ma	$\lambda\tau$	$\sigma_\lambda\tau$
F01	2048^3	0.10	8028	803	0.081	0.0320	0.0046
F005	2048^3	0.05	7959	398	0.080	0.0192	0.0029
F0025	2048^3	0.025	8050	201	0.081	0.0108	0.0026
F001875	2048^3	0.01875	8093	152	0.082	0.0039	0.0027
F00125	2048^3	0.0125	8171	102	0.082	-0.0004	0.0022
F001	2048^3	0.01	8178	82	0.082	-0.0009	0.0033
F0005	2048^3	0.005	8217	41	0.083	-0.0162	0.0035
FG00125	2048^3	0.0125	12580	157	0.084	0.0026	0.0015
FG001	2048^3	0.01	12313	123	0.082	-0.0041	0.0021
FG0005	2048^3	0.005	12415	62	0.083	-0.0146	0.0039
G00125	4096^3	0.0125	18391	229	0.093	0.0372	0.0063
G001	4096^3	0.01	18200	182	0.092	0.0065	0.0062
G000625	4096^3	0.00625	16126	101	0.081	-0.0049	0.0069
G0005	4096^3	0.005	16071	80	0.081	-0.0152	0.0008
H0005	4096^3	0.005	32930	165	0.083	0.0103	0.0019
H00031	4096^3	0.003125	32717	102	0.082	0.0021	0.0052
H00025	4608^3	0.0025	32910	82	0.083	-0.0097	0.0035

4 Table of spectral properties of a subset of the runs

Supplementary Table 2: Selected runs with spectral properties.

Pr_M	Re	Re_M	k_ν	k_{bs}	k_b	k_M	k_η	α_b
1.000000	1022	1022	157	11	21	56	157	-1.30
1.000000	2053	2053	268	16	36	100	268	-1.43
1.000000	4069	4069	456	22	62	173	456	-1.38
0.800000	1012	810	157	11	21	48	132	-1.29
0.800000	3998	3198	444	22	62	146	376	-1.40
0.400000	1014	405	156	11	21	35	78	-1.30
0.400000	4087	1634	459	22	62	105	231	-1.38
0.200000	1013	202	157	11	21	24	47	-1.29
0.100000	1018	101	157	11	21	16	27	-1.29
0.080000	1015	81	157	11	21	14	23	-1.29
0.080000	4068	325	451	22	62	41	67	-1.39
0.050000	4086	204	458	22	62	31	48	-1.38
0.050000	7958	397	755	32	101	50	79	-1.41
0.040000	2033	81	266	16	36	15	23	-1.44
0.020000	4038	80	449	22	62	16	23	-1.39
0.012500	8167	102	766	32	101	19	28	-1.41
0.012500	12580	157	1026	50	137	27	38	-1.39
0.012500	18391	229	1332	45	173	33	49	-1.48
0.010000	12313	123	1013	49	137	22	32	-1.39
0.010000	18200	182	1388	45	183	30	43	-1.48
0.006250	16126	100	1291	48	173	19	28	-1.45
0.005000	8217	41	767	32	101	10	14	-1.41
0.005000	12415	62	1013	49	137	13	19	-1.39
0.005000	16044	80	1273	45	165	16	23	-1.46
0.005000	32930	164	2037	97	264	26	38	-1.39
0.003125	32717	102	2036	100	272	19	26	-1.38

Pr_M is the magnetic Prandtl number, Re and Re_M are the fluid and magnetic Reynolds numbers, respectively. $k_\nu = (\epsilon_K/\nu^3)^{1/4}$ is the viscous dissipation wavenumber with the viscous dissipation rate ϵ_K. k_b and k_{bs} locate the maximum of the bottleneck and its starting point (75% of the maximum), respectively. $k_M = \int_k E_{mag}(k)k\,dk / \int_k E_{mag}(k)dk$ is the characteristic magnetic wavenumber. $k_\eta = k_\nu Pr_M^{3/4}$ is the ohmic dissipation wavenumber and α_b is the slope of the low-wavenumber part of the bottleneck. All wavenumbers in units of k_1.

5   Details of fitting procedures and error calculation

5.1   Growth rates

The growth rate λ is calculated from the time series of $B_{\rm rms}$ of the hydrodynamically saturated stage. For this, we fit $B_{\rm rms}(t)$ with $\exp(\lambda t)$ using a least-χ^2 fit. For a small number of runs, mostly at $\Pr_{\rm M} \approx 1$, we need to exclude that part of the time series, where no longer $B_{\rm rms} \ll \sqrt{\rho u_{\rm rms}^2}$ holds, i.e. the kinematic stage is left. The majority of runs always stays in the kinematic stage though. The error of the growth rate, σ_λ, is estimated from the maximum deviation of the fit, which is determined as follows: the time series is divided into three equal parts, each fitted to obtain its value λ_i, $i = 1, \ldots, 3$. We then use half the maximum difference to λ for the error, i.e. $\sigma_\lambda = \max |\lambda_i - \lambda|/2$. The minimal length of the time series was chosen to guarantee that σ_λ is small enough while the maximum is bound by the resolution, hence the computational cost. For resolutions of $256^3 - 512^3$, we have $t_{\rm max}/\tau \approx 500$, for $1024^3 - 2048^3$, $t_{\rm max}/\tau \approx 150$ and for 4096^3, $t_{\rm max}/\tau \approx 15$. λ and its error σ_λ are listed in Supplementary Table 1.

5.2   Critical magnetic Reynolds number

To calculate the critical magnetic Reynolds number $\mathrm{Re}_{\rm M}^{\rm crit}$ for each $\Pr_{\rm M}$ set, we fit a logarithmic function to the growth rate, i.e. $\lambda\tau = C_1 \ln(\mathrm{Re}_{\rm M}) + C_2$. This functional form is motivated by the theoretical expectation of [4, 1] and also by the distribution of the growth rates in Fig. 3a. We again use a least-χ^2 fit, but take into account the growth rate errors, σ_λ, for the weights. It turns out that the pre-factor C_1 varies between 0.017 and 0.028 with a mean of 0.022. Thus, we conclude that the chosen functional form is appropriate. $\mathrm{Re}_{\rm M}^{\rm crit}(\Pr_{\rm M})$ is calculated analytically from the zero of the fitting function, $\mathrm{Re}_{\rm M}^{\rm crit} = \exp(-C_2/C_1)$, and its error $\sigma_{\mathrm{Re}_{\rm M}^{\rm crit}}$ is derived directly from each fit, representing a one-sigma uncertainty of $\mathrm{Re}_{\rm M}^{\rm crit}$. The values and errors of $\mathrm{Re}_{\rm M}^{\rm crit}$ are then used in Fig. 3b and are listed in Supplementary Table 3 together with C_1. For the relative error $\sigma_{\mathrm{Re}_{\rm M}^{\rm crit}}/\mathrm{Re}_{\rm M}^{\rm crit}$, one finds for most of the runs values around $10 - 20\%$. However, taking these errors into account the decrease of $\mathrm{Re}_{\rm M}^{\rm crit}$ as function of $\Pr_{\rm M}$ is still significant.

Supplementary Table 3:   Critical magnetic Reynolds number

$\Pr_{\rm M}$	$\mathrm{Re}_{\rm M}^{\rm crit}$	$\sigma_{\mathrm{Re}_{\rm M}^{\rm crit}}$	C_1
1.0000	32	1.0	0.028
0.4000	60	2.6	0.025
0.2000	101	10.1	0.017
0.1000	150	11.7	0.021
0.0800	153	21.1	0.025
0.0500	153	13.4	0.021
0.0250	138	15.3	0.024
0.0125	119	49.8	0.018
0.0100	136	31.8	0.017
0.0050	108	18.5	0.022
0.003125	102	-	-

$\mathrm{Re}_{\rm M}^{\rm crit}$ is the critical magnetic magnetic Reynolds number obtained by a fit $\lambda\tau = C_1 \ln(\mathrm{Re}_{\rm M}/\mathrm{Re}_{\rm M}^{\rm crit})$ to the growth rate and $\sigma_{\mathrm{Re}_{\rm M}^{\rm crit}}$ its error. The last row refers to the only run for $\Pr_{\rm M} = 0.003125$ with $\lambda \approx 0$, hence $\mathrm{Re}_{\rm M} \approx \mathrm{Re}_{\rm M}^{\rm crit}$ (no fit).

5.3   Other fits

To obtain $\mathrm{Re}_{\rm M}^{\rm crit}(\Pr_{\rm M}) \propto \Pr_{\rm M}^{0.125}$ in Fig. 3b, we use also a least-χ^2 fit, employing the errors $\sigma_{\mathrm{Re}_{\rm M}^{\rm crit}}$, similar for $k_{\rm M}/k_\nu \propto \Pr_{\rm M}^\alpha$ in Fig 4.
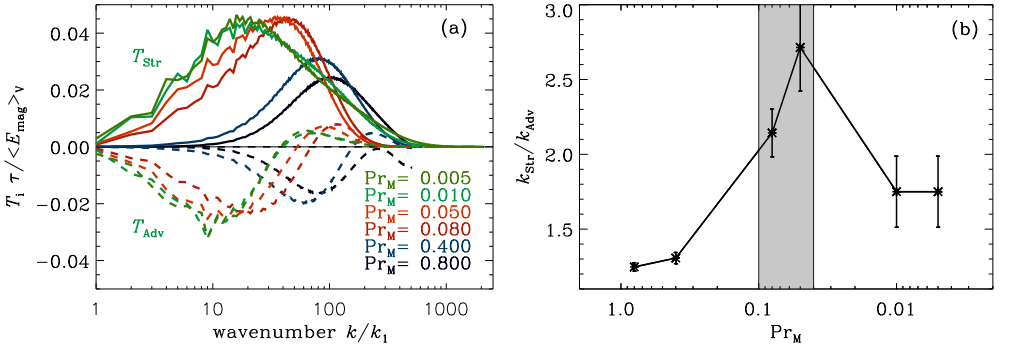
6   Magnetic energy transfer functions

Seeking further insight into the dynamo operating in the three regimes of Pr_M, we look at the spectral magnetic energy transfer functions. We follow the approach of [2], but using the convention by [3], where the contribution of compressibility is subsumed in the stretching/shearing and advection terms, T_{Str} and T_{Adv}, respectively, as follows

$$T_{Str}(\boldsymbol{k}) = \hat{\boldsymbol{B}}(\boldsymbol{k}) \cdot \widehat{(+\boldsymbol{B} \cdot \boldsymbol{\nabla u} - \boldsymbol{B} \boldsymbol{\nabla} \cdot \boldsymbol{u}/2)}^{*}(\boldsymbol{k})/2\mu_0 + \text{c.c.} \tag{1}$$

$$T_{Adv}(\boldsymbol{k}) = \hat{\boldsymbol{B}}(\boldsymbol{k}) \cdot \widehat{(-\boldsymbol{u} \cdot \boldsymbol{\nabla B} - \boldsymbol{B} \boldsymbol{\nabla} \cdot \boldsymbol{u}/2)}^{*}(\boldsymbol{k})/2\mu_0 + \text{c.c.} \tag{2}$$

Here, the hats indicate the Fourier transform and c.c. refers to the complex conjugate expressions. In Supplementary Fig. 4a, we show these functions after shell integration, i.e. as functions of $k = |\boldsymbol{k}|$, for six runs with $0.005 \leq Pr_M \leq 0.8$. As expected, the curves peak at higher wavenumbers for higher Pr_M. We also look at the ratio of the wavenumbers at which T_{Str} and T_{Adv} has its maximum and minimum, respectively, k_{Str}/k_{Adv}, which is determined from the curves after smoothing. We find that this ratio is maximal where the dynamo is hardest to excite, shown as grey shade in the Supplementary Fig. 4b. However, we should note that the simulations with the two lowest Pr_M have a higher resolution than the other four, which could also influence the result. It remains unclear whether, or how, this enhanced ratio would relate to the difficulty in exciting the dynamo at $0.1 \geq Pr_M \geq 0.04$.

Supplementary Figure 4: Shell integrated spectral magnetic energy transfer functions vs. magnetic Prandtl number Pr_M. Panel a: transfer by stretching/shearing, T_{Str}, and by advection, T_{Adv}, normalized by the total magnetic energy density $\langle E_{mag} \rangle_V = \int_k E_{mag}(k)\,dk$ divided by turnover time τ and averaged over time. Color coding refers to Pr_M as shown in the legend. Panel b: ratio of the wavenumbers of maximal stretching and minimal advection, k_{Str}/k_{Adv}, as a function of Pr_M. The grey shaded area indicates the interval $0.1 \geq Pr_M \geq 0.04$, where the dynamo is hardest to excite. The errors are calculated using an estimated uncertainty in determining k_{Str} and k_{Adv}, Used runs: E08, E04, E008, E005, G001, H0005.

7 Numerical diffusivity

In our low $\Pr_M$ simulations, $\eta \gg \nu$, hence numerical diffusion might only play a role for the velocity field. We estimate the numerical viscosity in our simulations in two ways. Firstly, we follow the approach of [2], to estimate the fluid Reynolds number from the power spectra. For this we determine the Taylor microscale

$$\lambda_{\mathrm{TM}} = \left(\int_k E_{\mathrm{kin}}(k)dk \,/ \int_k k^2 \, E_{\mathrm{kin}}(k)dk \right)^{1/2}, \tag{3}$$

and the integral scale for turbulent motions

$$\lambda_{\mathrm{int}} = \int_k k^{-1} E_{\mathrm{kin}}(k)dk \,/ \int_k E_{\mathrm{kin}}(k)dk. \tag{4}$$

These scales can be used to estimate the effective Reynolds number as

$$\mathrm{Re}_{\mathrm{eff}} \propto (\lambda_{\mathrm{int}}/\lambda_{\mathrm{TM}})^2. \tag{5}$$

This is often used to estimate $\mathrm{Re}_{\mathrm{eff}}$ from observations or in simulations that use only numerical diffusivities, although the proportionality constant is unknown. As shown in Supplementary Fig. 5, the effective Re based on Equation (5) scales linearly with Re based on the prescribed value of ν. Assuming now plausibly numerical diffusion to enter mainly in the form of hyperdiffusion, we infer that from this linear relationship a notable influence of numerical diffusion can be ruled out.
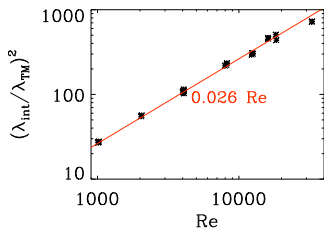
Supplementary Figure 5: Effective Reynolds number proxy (5) as a function of Re from the prescribed ν. The red line indicates $(\lambda_{\mathrm{int}}/\lambda_{\mathrm{TM}})^2 = 0.026 \, \mathrm{Re}$.

In addition, we performed a flow decay experiment to estimate the numerical diffusion from the flow decay rate in the absence of all other terms. The resulting effective viscosity is to high precision the same as the prescribed ν up to wavenumbers $k \lesssim 1000 \, k_1$, covering safely all scales relevant for the magnetic field. From these two results we conclude that our numerical simulations are not affected by numerical diffusion, and that the $\Pr_M$ regimes are accurately identified.

References

[1] N. KLEEORIN AND I. ROGACHEVSKII, *Growth rate of small-scale dynamo at low magnetic Prandtl numbers*, Phys. Scr, 86 (2012), p. 018404.

[2] J. PIETARILA GRAHAM, R. CAMERON, AND M. SCHÜSSLER, *Turbulent Small-Scale Dynamo Action in Solar Surface Simulations*, ApJ, 714 (2010), pp. 1606–1616.

[3] M. REMPEL, *Numerical Simulations of Quiet Sun Magnetism: On the Contribution from a Small-scale Dynamo*, ApJ, 789 (2014), p. 132.

[4] I. ROGACHEVSKII AND N. KLEEORIN, *Intermittency and anomalous scaling for magnetic fluctuations*, Phys. Rev. E, 56 (1997), pp. 417–426.